

Numerical investigations of holographic imaging quality*

JERZY NOWAK, MAREK ZAJĄC

Institute of Physics, Technical University of Wrocław, Wybrzeże Wyspiańskiego 27,
50-370 Wrocław, Poland.

While making use of the previously worked out numerical method of determining light intensity distribution in the holographic image, the quality of imaging for two chosen examples of holographic recording and reconstruction geometries were analysed. Beside the images of one- and two-point objects, the images of extended objects such as edge, Ronchi ruling and sinusoidal amplitude test were studied, which enabled a complex evaluation of holographic imaging quality.

1. Introduction

Evaluation of imaging quality is one of the problems appearing in holography. The easiest method to do it is to determine the III and V order aberration coefficients [1-3]. It is also possible to determine wave aberration [4], or to obtain by "ray tracing" method a spot-diagram from which aberration spot could be inferred [5,6]. Since, however, in holography, most often coherent light is used (and our considerations will be limited to this case only) then the distribution of the light intensity, essential for the analysis of imaging quality, cannot be deduced from spot-diagrams. For the above reason a numerical method for determining the light intensity distribution in the holographic image of a point-object, i.e., in the aberration spot, was developed and presented in [7, 8]. Since in the case of coherent light it is not enough to know aberration spot only, hence it has been proposed to calculate the light intensity distribution in the image of a two-point object [9]. It allowed us to determine a resolution limit since this parameter is recognized as one of the popular imaging quality measures.

Based on the numerically calculated complex point spread function (and assuming isoplanatism which is usually taken) it is possible to determine the light intensity distribution in the image of an extended object

$$I(x_3) = \left| \int t(x)h(x-x_3)dx \right|^2 \simeq \left| \sum_j t(x_j)h(x_j-x_3) \right|^2 \quad (1)$$

* This work was carried on under the Research Project M.R. I.5, and presented at the VI Polish-Czechoslovak Optical Conference, Lubiatów (Poland), September 25-28, 1984.

where t — amplitude transmittance of the object,
 h — complex point spread function,
 x_s — coordinate in the image plane.

For the sake of convenience and shortening the computing time, the problem is treated here one-dimensionally. This method was applied in the paper [10] to analysis of imaging given by a holographic lens. In this paper the subject of the analysis is holographic imaging investigated on the example of two typical geometries of the hologram recording and image reconstruction. From the formula (1) the light intensity distribution is determined for the following extended objects: edge, Ronchi ruling and sinusoidal amplitude grating. For comparison, light intensity distributions were determined in the aberration spot and in the image of two-point objects.

2. Numerical results

2.1. In-line hologram

The parameters of hologram recording and image reconstruction are given in Table 1 (example No. 1). Symbols P, R and C denote object wave, reference wave and reconstruction wave, respectively, z is the distance measured along the axis perpendicular to the hologram, and x is the distance from this axis.

Table 1. Geometry of hologram recording and image reconstruction

Example number	P	R	C
1	$x_1 = \begin{cases} 0 \\ 5 \end{cases}$ $z_1 = -100$	$x_R = 0$ $z_R = -200$	$x_C = 0$ $z_C = -120$
2	$x_1 = \begin{cases} -5 \\ 0 \\ 5 \end{cases}$ $z_1 = 100$	$x_R = 10$ $z_R = -100$	$x_C = 10.4$ $z_C = -100$

All values in the Table are given in millimeters.

It has been assumed, that the wavelength during recording and reconstruction does not change and that the hologram is not overscaled ($\mu = m = 1$). The diameter of hologram equals 10 mm. The geometry of image reconstruction was chosen so ($z_C \neq z_R$) that the reconstructed image be charged with aberrations. Two cases were analysed: one for the field $x_1 = 0$ and the other for the

field $x_1 = 5$. Figure 1 presents normalized light intensity distribution in both the aberration spots. The position of the image in this figure, as well as in all other ones, is referred to the position of the Gauss image. It can be seen that the image of the point lying outside the axis is asymmetrical due to the field aberrations.

Figure 2 shows the energy distribution in the aberration spots, which allows

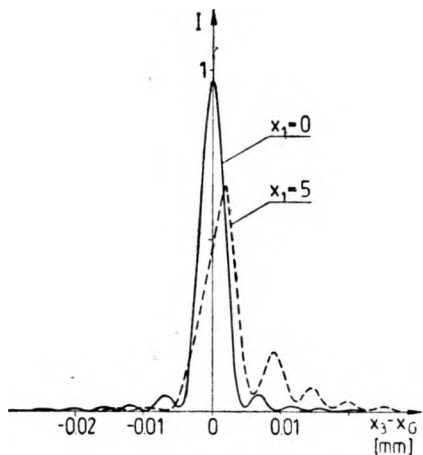


Fig. 1. Light intensity distribution in aberration spot for various values of the field angle. Example No. 1

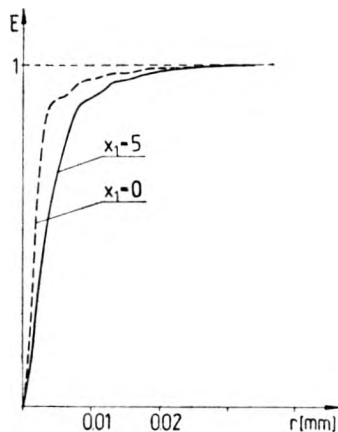


Fig. 2. Energy distribution in aberration spot for various values of the field angle. Example No. 1

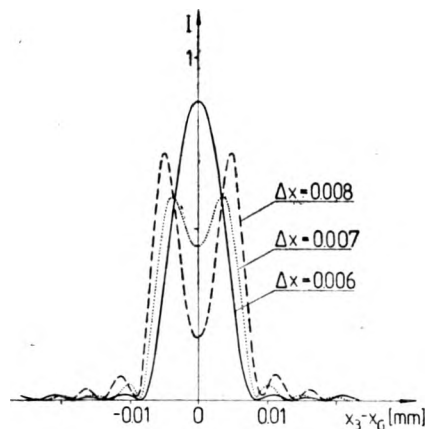


Fig. 3. Light intensity distribution in the image of two-point object ($x_1 = 0$ mm). Example No. 1

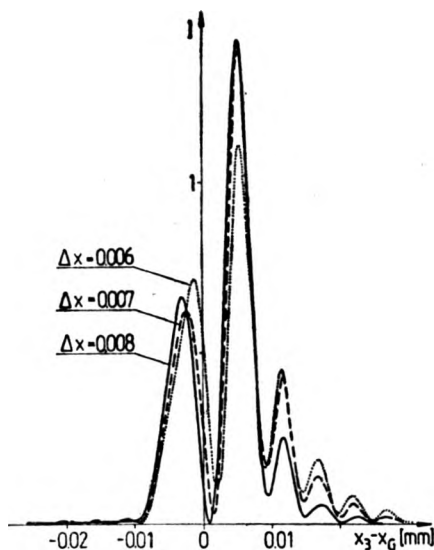


Fig. 4. Light intensity distribution in the image of two-point object ($x_1 = 5$ mm). Example No. 1

us to estimate the size of these spots, defined by the diameter of a circle containing 80 % of total energy. For $x_1 = 5$ mm it is distinctly greater than for $x_1 = 0$.

Figure 3 presents the light intensity distribution in the images of two-point objects lying on the axis. Δx is the distance between the object points. It allows us to estimate the resolution limit. It may be assumed that in this case $\Delta x = 0.007$ mm. Analogical plots, but for the objects lying beyond the axis ($x_1 = 5$ mm) are given in Fig. 4. In this case the light intensity distributions are much more complicated and it is more difficult to determine the resolution limit. It seems, however, that it is $\Delta x = 0.008$ mm.

The parameters describing numerically the aberration spot are presented in Table 2 (example No. 1). In the respective columns the following quantities are given: maximum light intensity in the aberration spot (I_{\max}), distance between the spot centre of gravity and the position of Gauss image ($\bar{x} - x_G$), second and third order moments of the light intensity distribution in the spot (M_2 and M_3), cf. [8], diameter of the circle containing 80 % of total energy ($d_{0.8}$), and, additionally, the value of the resolution limit (Δx). The third order moment of the light intensity distribution is, as it is known, the measure of the spot's symmetry, thus for $x_1 = 0$, $M_3 = 0$.

Table 2. Parameters determining aberration spot

Example number	x_1	I_{\max}	$\bar{x} - x_G$	M_2	M_3	$d_{0.8}$	Δx
1	0	0.97	0	1.7×10^{-5}	0	0.006	0.007
	5	0.61	0.003	3.6×10^{-5}	2.2×10^{-7}	0.013	0.008
2	-5	0.65	0.005	4.1×10^{-5}	1.2×10^{-7}	0.016	0.006
	0	0.83	0.006	3.0×10^{-5}	1.3×10^{-7}	0.011	0.010
	5	0.94	0.004	2.2×10^{-5}	1.3×10^{-8}	0.008	0.004

All values in the Table are given in millimeters

The results gathered in Table 1, as well as the curves presented in Figs. 1-4, suggest — according to our expectations — that imaging outside the axis is worse than for $x_1 = 0$. This conclusion ought to be confronted with those that the analysis of the images of the extended objects.

The images of an edge are presented in Fig. 5. The influence of aberrations is distinctly seen here for $x_1 = 5$ mm. The images of Ronchi ruling of the chosen spatial frequencies ν equal to 20 l/mm, 80 l/mm and 120 l/mm, are presented in Figs. 6-8, respectively. It may be seen that for the image on the axis ($x_1 = 0$) Ronchi ruling of the frequency $\nu = 120$ l/mm is practically not transferred, whereas for $x_1 = 5$ mm the imaging is much better.

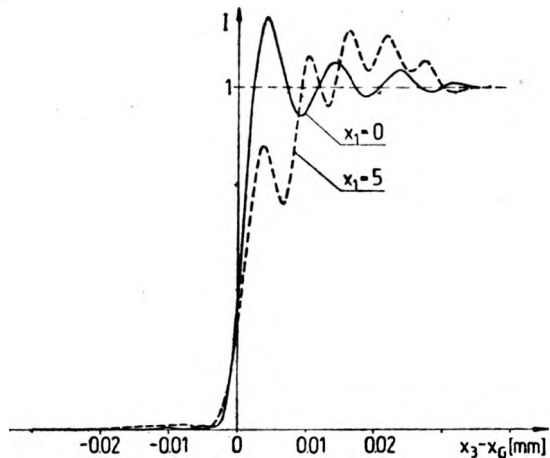


Fig. 5. Image of an edge for various values of the field area. Example No. 1

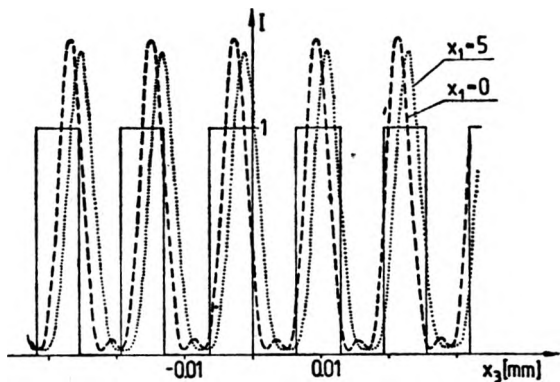


Fig. 7. Image of Ronchi ruling of spatial frequency $\nu = 80$ l/mm for various values of the field angle. Example No. 1

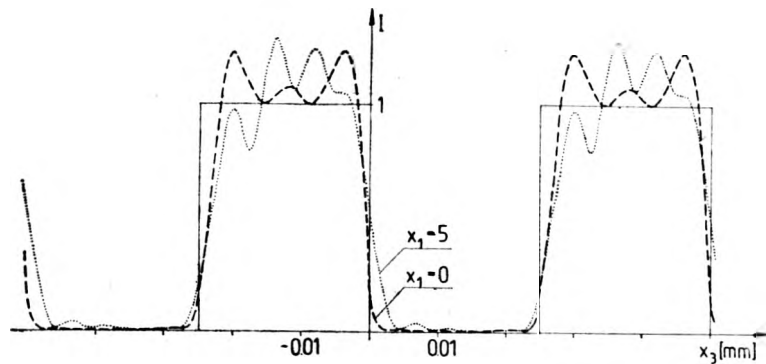


Fig. 6. Image of Ronchi ruling of spatial frequency $\nu = 20$ l/mm for various values of the field angle. Example No. 1

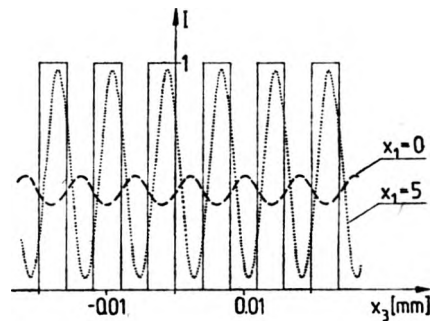


Fig. 8. Image of Ronchi ruling of spatial frequency $\nu = 120$ l/mm for various values of the field area. Example No. 1

Conclusions, referring to imaging quality, which may be drawn by analysing the images of Ronchi ruling are thus contrary to those inferred from the analysis of point-object images. This effect is even better seen in Fig. 9, which presents the contrast in the image of sinusoidal object (of contrast equal to 1) vs. spatial frequency. The cut-off frequency resulting from diffraction limitation equals 180 l/mm , whereas for $x_1 = 0$ the contrast of the image drops practically

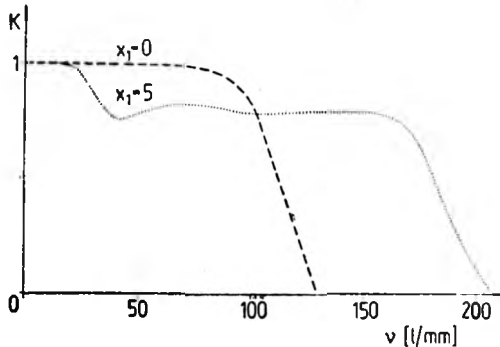


Fig. 9. Contrast in the image of amplitude sinusoidal test vs. spatial frequency for various values of field angle. Example No. 1

to zero at the frequency as low as of about 120 l/mm , and for $x_1 = 5 \text{ mm}$ it does not decrease below 0.8 up to about 170 l/mm .

2.2. Quasi-Fourier hologram

For this case the conditions of the hologram recording and image reconstruction are presented in Table 1, as the example No. 2. The sources of reference and reconstructing waves lie in the same plane ($z_R = z_O$), but at different distances from the axis ($x_R \neq x_O$), that is why the image is burdened with aberrations. The investigations were performed for the objects positioned in points $x_1 = 0$, $x_1 = 5 \text{ mm}$ and $x_1 = -5 \text{ mm}$, since in the case of an off-axis reference beam the, symmetry with respect to the z axis is lacking.

Analogical diagrams to those given for the previous example are presented graphically in the Figs. 10–19. From the analysis of aberration spot, presented in Fig. 10, it follows, that the best imaging occurs for $x_1 = 5 \text{ mm}$. The imaging of point-objects situated in points $x_1 = 0$ or $x_1 = -5 \text{ mm}$ are worse. It is confirmed by Fig. 11, in which the energy distribution in aberration spot is presented. The diameter of spot containing 80% of total energy is the smallest for $x_1 = 5 \text{ mm}$.

The following three figures (Figs. 12-14) present light intensity distribution in the images of two-point objects of different inter-point distances Δx , which allowed us to determine the resolution limit in the way given is the previous example.

Parameters characterizing the aberration spot and the resolution limit are given in Table 2 (example No. 2). From the analysis of the point-object imaging it results undoubtedly that the best imaging occurs for $x_1 = 5$ mm.

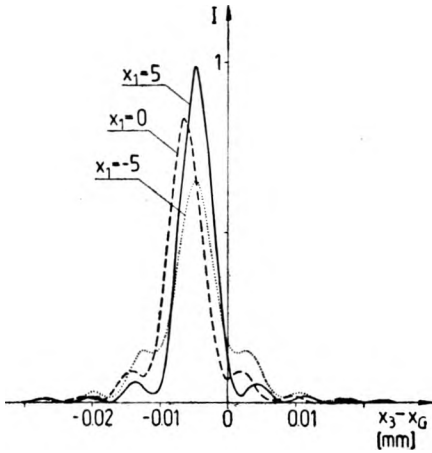


Fig. 10. Light intensity distribution in aberration spot for various values of the field area. Example No. 2

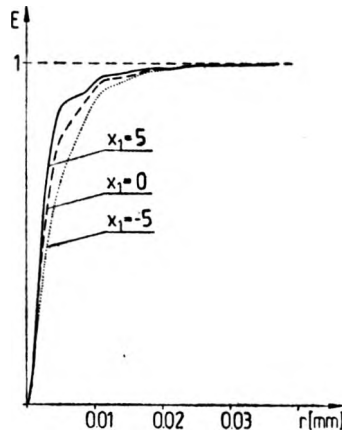


Fig. 11. Energy distribution in aberration spot for various values of the field angle. Example No. 2

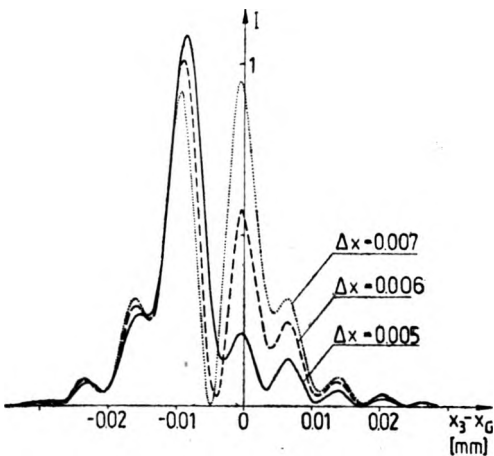


Fig. 12. Light intensity distribution in the image of two-point object ($x_1 = -5$ mm). Example No. 2

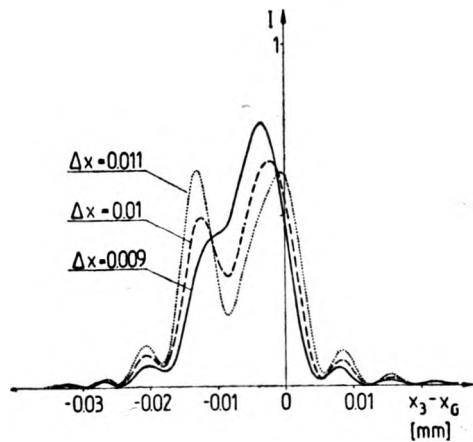


Fig. 13. Light intensity distribution in the image of two-point object ($x_1 = 0$). Example No. 2

Further analysis refer to extended objects. Figure 15 presents the images of an edge. (The curve for $x_1 = 5$ mm could not be included because of high values of light intensity in the local maxima, which would make it necessary to change the scale, the figure being all the same scarcely comprehensible).

The images of the Ronchi ruling for the same spatial frequencies as in the first case are presented in Figs. 16–18. It can be seen that the test of frequency

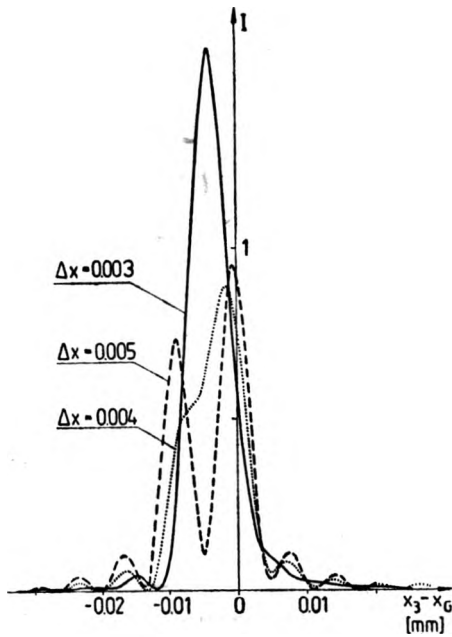


Fig. 14. Light intensity distribution in the images of two-point objects ($x_1 = 5$ mm). Example No. 2

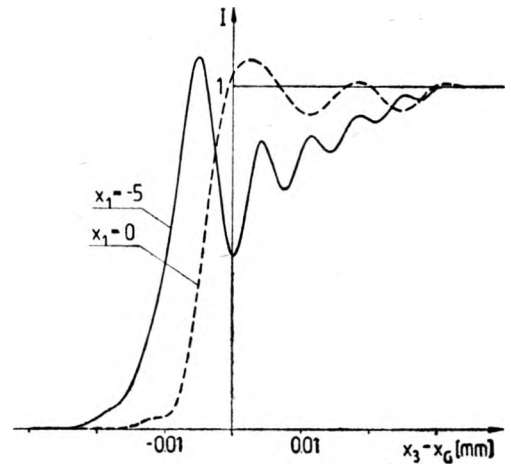


Fig. 15. Image of an edge for various values of the field angle. Example No. 2

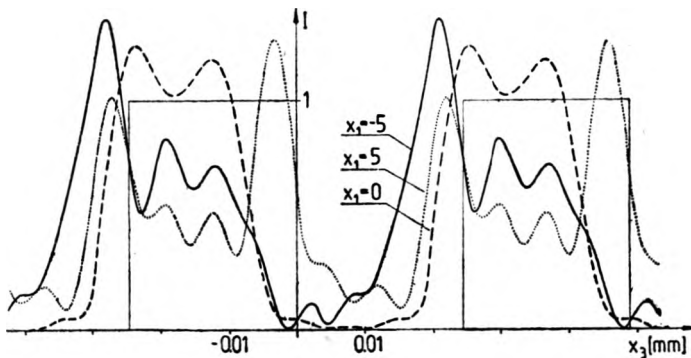


Fig. 16. Image of Ronchi ruling of spatial frequency $\nu = 20$ l/mm for various values of the field angle. Example No. 2

$\nu = 120 \text{ l/mm}$ is best imaged for $x_1 = 0$, whereas for $x_1 = -5 \text{ mm}$ the test of the frequency $\nu = 160 \text{ l/mm}$ is imaged with the contrast nearly equal to 1.

Similarly as in the example 1, the conclusions referring to the quality of imaging, based on the analysis of extended objects imaging, do not agree with those resulting from the analysis of one-and two-point objects.

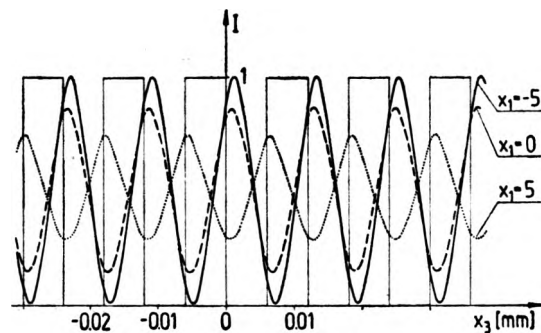


Fig. 17. Image of Ronchi ruling of spatial frequency $\nu = 80 \text{ l/mm}$ for various values of the field angle. Example No. 2

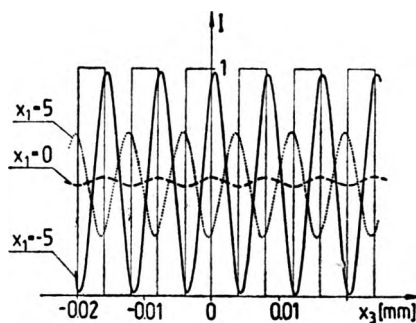


Fig. 18. Image of Ronchi ruling of spatial frequency $\nu = 120 \text{ l/mm}$ for various values of the field angle. Example No. 2

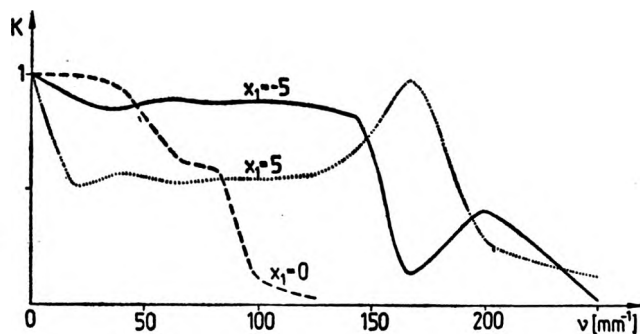


Fig. 19. Contrast in the image of amplitude sinusoidal test vs. spatial frequency for various values of the field angle. Example No. 2

3. Final conclusions

Summing up, it should be stated that a full evaluation of holographic imaging quality cannot be based on analyses of only one- and two-point objects, like in the case of classical optics. The method proposed allows us to determine the image characteristics of simple extended objects of which the amplitude sinusoidal grating seems to be the most important. It should be noted, however, that since we deal with the imaging in coherent light, the value of the contrast in the image of such test has essentially different meaning than this in incoherent light (in particular, it is not possible to determine the Contrast Transfer Function).

References

- [1] MEIER R. W., J. Opt. Soc. Am. **56** (1965), 987.
- [2] CHAMPAGNE E. B., J. Opt. Soc. Am. **57** (1967), 51.
- [3] LATTA J. N., Appl. Optics **10** (1967), 666.
- [4] MILES J. F., Optica Acta **20** (1973), 19.
- [5] OFFNER A., J. Opt. Soc. Am. **56** (1966), 1509.
- [6] NOWAK J., ZAJĄC M., Optik **55** (1980), 93.
- [7] NOWAK J., ZAJĄC M., Optica Applicata **12** (1982), 250.
- [8] NOWAK J., ZAJĄC M., Optica Acta **13** (1983), 1749.
- [9] NOWAK J., ZAJĄC M., Optica Applicata **14** (1984).
- [10] NOWAK J., ZAJĄC M., *Numerical investigations of the imaging by holographic lens* (in print in Optik).

Received December 4, 1984

Численные исследования качества голографического отображения

При использовании уже разработанного численного метода определения интенсивности света в голографическом изображении было исследовано качество отображения для двух избранных примеров голографической регистрации и реконструкции. Независимо от исследования изображений одно- и двухпунктирных предметов было исследовано отображение таких предметов как: кант, тест Рончи и синусоидальная, амплитудная сетка. Это делает возможной комплексную оценку качества голографического отображения.